Journal of Electron Spectroscopy and Related Phenomena 193 (2014) 1–5

Contents lists available at ScienceDirect

Journal of Electron Spectroscopy and Related Phenomena

journal homepage: www.elsevier.com/locate/elspec

High resolution (e, 2e) spectroscopy of dimethyl ether

Y.R. Miao[a,b], J.M. Li[a,b], J.K. Deng[a], C.G. Ning[a,b,*]

[a] Department of Physics, State Key Laboratory of Low-Dimensional Quantum Physics, Tsinghua University, Beijing 100084, China
[b] Collaborative Innovation Center of Quantum Matter, Beijing, China

ARTICLE INFO

Article history:
Received 18 September 2013
Received in revised form
30 December 2013
Accepted 28 January 2014
Available online 7 February 2014

Keywords:
(e, 2e)
Dimethyl ether
Dyson orbital
SAC-CI

ABSTRACT

We report high-resolution (e, 2e) spectra of dimethyl ether (H_3COCH_3) in combination with high-level theoretical calculations. The observed binding energy spectra and momentum distributions were compared with Hartree–Fock, density functional theory (DFT), and symmetry-adapted-cluster configuration-interaction (SAC-CI) calculations. In general, the theoretical momentum distributions based on Dyson orbital (DO) and Kohn–Sham orbital (KSO) agree well with the experimental momentum distributions except the discrepancies in the low momentum regions of $2b_1$ and $1a_2$ orbitals. The present high resolution experimental data provide a benchmark for the future rigorous theories.

1. Introduction

Electron impact ionization collisions are important for many fundamental areas, such as plasmas, radiation damage of living tissues [1]. The kinetically complete (e, 2e) experiments can provide the benchmark data against the electron collision theories and the electronic structure theories [2,3]. However, the low resolution and low statistical accuracy of most (e, 2e) experiments cannot provide rigorous test for various theories. In the present work, we report the high-resolution (e, 2e) experiment of dimethyl ether. Dimethyl ether, the simplest ether, is a colorless gas, which is widely used as a precursor for other compounds and an aerosol propellant. Its electronic structures have been extensively investigated using ultra-violet ray [4], He I and He II photoelectron spectroscopy (PES) [5–9]. The first (e, 2e) studies on dimethyl ether were reported by Clark et al. [10], and then by Zheng et al. [11]. In both studies, significant discrepancies were observed between the experimental momentum distributions and the theoretical predictions of its valence orbitals. The discrepancies observed in previous studies were ascribed by Zheng et al. [11] to the quite small basis set and neglecting electron correlation effects in calculations. However, the explanation is not conclusive since their rather poor energy resolution (1.3 eV) cannot resolve each state. In the present work, we employed a basis set approaching the basis set limit and a high level many-body theory for rigorously comparing with the high resolution (e, 2e) experiment [12,13]. To test the plane wave impulsive approximation (PWIA) [14–16], the experiment was conducted at two different impact energies 600 and 1200 eV.

The spectrometer used in the present work is our 3rd generation high-resolution electron momentum spectrometer [13]. The energy resolution is 0.7 eV (full width at half maximum, FWHM). The acceptance of the polar angle θ is $\pm 0.53^\circ$, and the azimuthal angle ϕ resolution is $\pm 0.84^\circ$. The gaseous sample of dimethyl ether with a purity of 99.9% was directly used without further purifications. No impurities were observed in the ionization potential spectra.

2. Theory and experimental methods

The spectrometer used in the present work takes the non-coplanar symmetric (e, 2e) configuration. The kinetic energies (E_1, E_2) and momenta (p_1, p_2) of two outgoing electrons are determined through the coincidence detection, while the energy (E_0) and momentum (p_0) of the incident electron are pre-defined. Under the high impact energy, and the large momentum transfer, the differential (e, 2e) cross-section can be factorized into the product of a structural factor and a kinematic term, while the later term is approximately constant. Therefore, under PWIA, the differential cross-section of (e, 2e) can be written as [14]

$$\sigma_{EMS} \propto S_i^f \int d\Omega \left| \left\langle e^{-ipr} \Psi_f^{N-1} \middle| \Psi_i^N \right\rangle \right|^2, \quad (1)$$

* Corresponding author at: Department of Physics, State Key Laboratory of Low-Dimensional Quantum Physics, Tsinghua University, Beijing 100084, China.
Tel.: +86 1062785594; fax: +86 1062781604.
E-mail address: ningcg@tsinghua.edu.cn (C.G. Ning).

0368-2048/$ – see front matter © 2014 Elsevier B.V. All rights reserved.
http://dx.doi.org/10.1016/j.elspec.2014.01.019

where S_i^f represents the spectroscopic factor, e^{-ipr} stands for the plane wave, the momentum p is determined by the azimuthal angle ϕ, Ψ_i^N and Ψ_f^{N-1} are the wave functions of the ground state and the ionized state of the target, respectively. N is the total electron number. $\int d\Omega$ represents the spherical average for the randomly oriented molecules in gas phase. The overlap integral $\langle\Psi_f^{N-1}|\Psi_i^N\rangle$ is called Dyson orbital [14,17–20], which can be calculated using the many-body theories, such as the configure interaction, or Green's function theory. In this sense, Dyson orbital is defined by the ionization process. The calculated Dyson orbital is usually constructed using the linear combination of Hartree–Fock orbitals. If the Ψ_f^{N-1} and Ψ_i^N are in the form of a single determinant, under the frozen orbital approximation, Eq. (1) can be simplified as

$$\sigma_{EMS} \propto S_i^f \int d\Omega |\varphi_j(p)|^2, \tag{2}$$

where $\varphi_j(p)$ is the jth molecular orbital in the momentum space, which can be a Hartree–Fock orbital (canonical molecular orbital, CMO)[14] or a Kohn–Sham orbital (KSO) [21].

In the present work, Dyson orbitals were calculated using the symmetry adapted cluster configuration interaction (SAC-CI) theory, which was originally developed by Hiroshi Nakatsuji [22]. The SAC-CI can calculate singlet, doublet, and up to septet excited state of molecules. The SAC-CI theory has been used to interpret the (e, 2e) binding energy spectra of furan, pyrrole, and thiophene [23], CS_2 [24], and CO_2 [25]. Recently, we introduced SAC-CI method to calculate momentum distributions of Dyson orbitals [26–28]. In the present SAC-CI calculations, ten occupied valence molecular orbitals and 120 unoccupied orbitals were included in the active space. Higher order linked operators R (more than triple) were generated by the exponential generation algorithm [22]. The highest R is specified by Max$R$ = 5. We calculated 250 cation doublet states for A_1, and 50 for other each irreducible representation (A_2, B_1, B_2) to reproduce the ionization potentials in the whole valence region. A home compiled program, ***NEMS***, was used to calculate the spherically averaged momentum distributions of Dyson orbitals [29]. The widely used B3LYP (Becke-3-parameter-Lee–Yang–Parr) hybrid exchange-correlation functional [30,31] was employed in the density functional theory (DFT) calculation.

Moreover, the outer valence Green's function (OVGF) method [32,33] was used to calculate the vertical ionization potential. Within the theoretical framework of DFT, the statistical average of orbital potentials method (SAOP) [34], and the so-called ΔB3LYP method [35] were also employed to predict the vertical ionization potential. ΔB3LYP stands for the total energy difference between the valence–hole cation and the neutral ground state of the molecule using DFT-B3LYP method. In present work, except SAOP and ΔB3LYP calculations which used the triple ζ and two-polarization (TZ2P) Slater-type basis set, all other calculations employed the Aug-cc-pVTZ Gaussian-type basis set [36].

3. Results and discussion

3.1. Ionization potential spectra

The geometry structure of dimethyl ether molecule is illustrated by the inset in Fig. 1(b). It has C_{2v} symmetry at equilibrium. Its electronic configuration at ground state can be written as

$$(\text{core})^6\underbrace{(3a_1)^2(2b_2)^2(4a_1)^2}_{\text{inner valence}}$$

$$\underbrace{(1b_1)^2(5a_1)^2(3b_2)^2(1a_2)^2(4b_2)^2(6a_1)^2(2b_1)^2}_{\text{outer valence}}.$$

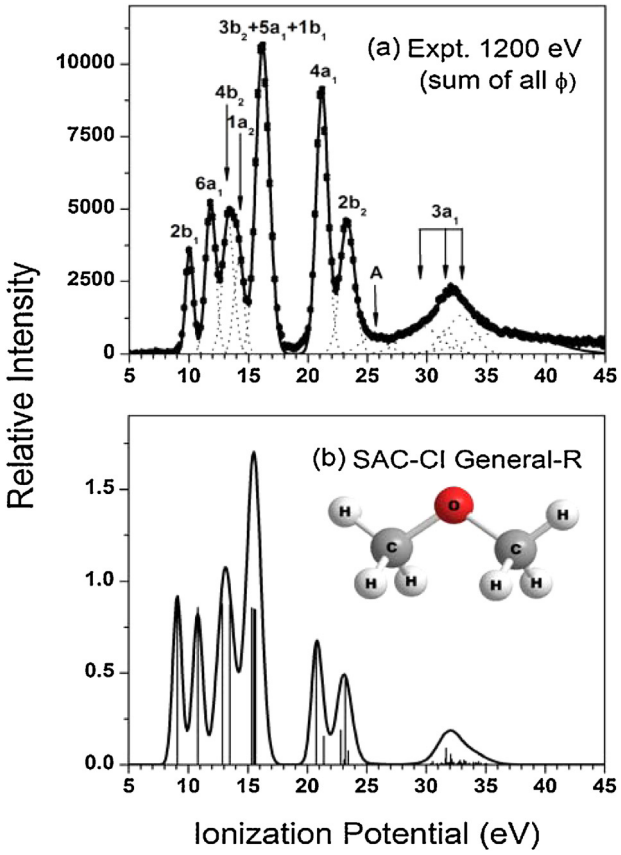

Fig. 1. Binding energy spectra of dimethyl ether. (a) The experimental (e, 2e) binding energy spectrum summed over all azimuthal angles ϕ. Twelve Gaussian peaks (dashed lines) were employed in the fitting procedure to extract the experimental momentum distribution for each orbital. The label A indicates an additional band, which cannot be predicted by SAC-CI calculations. (b) The simulated binding energy spectrum using SAC-CI General-R method. The positions of the vertical spikes represent the ionization potentials while their heights stand for the spectroscopic factors. The inset shows the molecular structure of dimethyl ether.

The experimental (e, 2e) ionization potential spectrum of dimethyl ether at the impact energy of 1200 eV plus binding energies is shown in Fig. 1(a). There are seven resolved ionization bands. The ionization potentials of the first four orbitals $2b_1$, $6a_1$, $4b_2$, and $1a_2$ are 10.1 eV, 11.8 eV, 13.3 eV, and 14.2 eV, respectively. The orbitals $3b_2$, $1b_1$, $5a_1$ are too close to be resolved. One fitting Gaussian function located at 16.2 eV was used to extract their summed experimental momentum distributions. The $4a_1$ and $2b_2$ orbitals located at 21.2 eV and 23.3 eV, respectively. The SAC-CI method predicts that the ionization from $4a_1$ and $2b_2$ will induce several satellite lines, as shown in Fig. 1(b). The broad band in the binding energy region of 30–35 eV in Fig. 1(a) is mainly attributed to the congested satellite lines of $3a_1$ orbital, as reproduced by SAC-CI. The observed band marked by A in Fig. 1(a) is consistent with the previous work by Zheng et al. [11], but cannot be predicted by our high level SAC-CI calculations. As shown in Fig. 1(b), there is no such a structure in the binding energy region of 25–29 eV in the simulated spectrum. Moreover, there is no evident peak A in HeII excited spectrum reported by Potts et al. [4] either. Except this minor discrepancy, in general, the SAC-CI calculation reproduced very well the main features of the experimental spectrum.

In Table 1, the experimental ionization potentials were compared with various theoretical predictions in detail. In addition to the SAC-CI, the SAOP, OVGF, and ΔB3LYP methods can also reproduce the ionization potentials for the outer valence orbitals with considerably less computational costs. However, for the inner

Table 1
Ionization potentials (eV) and spectroscopic factors (in parentheses) of dimethyl ether.

	EMS[a]	PES[b]	SAC-CI[a]	SAOP[a]	OVGF[a]	ΔB3LYP[a]
$2b_1$	10.1 (0.86)	10.1	9.08 (0.861)	10.67	10.29 (0.924)	9.87
$6a_1$	11.8 (0.87)	11.9	10.79 (0.857)	12.16	12.04 (0.923)	11.50
$4b_2$	13.3 (0.88)	13.4	12.86 (0.874)	13.52	13.75 (0.922)	13.10
$1a_2$	14.2 (0.75)	14.2	13.48 (0.872)	13.96	14.32 (0.921)	13.59
$3b_2$	16.2 (0.855)[c]		15.32 (0.855)	15.60	16.11 (0.914)	15.65
$5a_1$	16.2 (0.849)[c]	16.2	15.51 (0.849)	16.02	16.37 (0.916)	15.66
$1b_1$	16.2 (0.845)[c]		15.66 (0.845)	16.08	16.43 (0.916)	15.72
$4a_1$	21.2 (0.65)	21.2	20.76 (0.648)	20.17	21.75 (0.888)	20.14
			21.39 (0.154)			
$2b_2$	23.3 (0.65)	23.4	22.80 (0.188)			
			23.07 (0.026)			
			23.20 (0.481)	22.25	24.03 (0.973)	22.42
			23.46 (0.074)			
A	25.5 (0.09)					
$3a_1$	30–35 (0.53)		30.54 (0.018)	30.54		31.46
			31.30 (0.010)			
			31.62 (0.033)			
			31.69 (0.090)			
			32.04 (0.056)			
			32.14 (0.030)			
			32.32 (0.014)			
			32.77 (0.017)			
			32.85 (0.025)			
			33.17 (0.024)			
			33.31 (0.012)			
			33.36 (0.018)			
			33.98 (0.013)			
			34.40 (0.016)			

[a] Present work. OVGF and SAC-CI calculations were performed using Gaussian03 [41], whereas SAOP and ΔB3LYP were done in ADF program [42]. Only the spectroscopic factors greater than 0.01 were listed here.
[b] From Ref. [5].
[c] The spectroscopic factors given by SAC-CI were directly used for normalizing the experimental momentum distributions.

valence orbitals, the three later approaches cannot predict the satellite structures.

3.2. Electron momentum distributions

In Fig. 2, the experimental momentum distributions of highest occupied molecular orbital (HOMO) $2b_1$ were compared with the theoretical momentum distributions generated using different models. The Kohn–Sham orbitals (KSOs) were generated using B3LYP functional, and Dyson orbitals (DO) were constructed using the SAC-CI general-R. The correlation-consistent basis set Aug-cc-pVTZ was used in the calculations. Since it usually produces more than one SAC-CI Dyson orbitals when ionizing one electron from an electronic state, especially for the inner valence orbitals, the Dyson orbital with the greatest spectroscopic factor was selected as the main orbital in comparisons. The band $3b_2 + 5a_1 + 1b_1$ is chosen for determination of the normalization because its experimental distributions can be well reproduced using SAC-CI method. Moreover, its intensity is strong and well separated from other orbital. Therefore, the contamination from neighboring orbitals can be excluded.

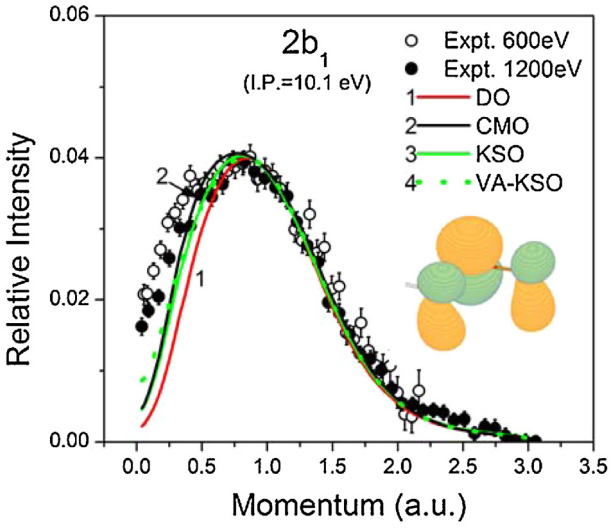

Fig. 2. Spherically averaged momentum distributions for the HOMO of dimethyl ether. The theoretical results have been convoluted with the experimental momentum resolution. The curve 4 is the vibrationally averaged DFT calculation. The inset shows Dyson orbital of $2b_1$ plotted with a contour value 0.05.

It can be seen that the predicted momentum profiles using CMO, KSO, and DO agree with the experimental distributions. However, there is a noticeable discrepancy in the lower momentum region ($p < 0.5$ a.u.). It should be noted that the discrepancy is unlikely due to the electron correlation effects as suggested by Zheng et al. [11] because the agreement became even worse when using KSO or DO orbitals. DFT-B3LYP method partly includes the electron correlation through the exchange-correlation functional, and SAC-CI takes into account the electron correlation both for the initial target and the final ion. Recently, Watanabe et al. [37] have shown that the nuclear ground vibrations may have effects on the momentum distributions. We indeed found that the ν_{18} mode (3039 cm^{-1}, see Fig. S1) has non-neglectable effect on the momentum distributions of HOMO after checking all vibrational modes. The vibrationally averaged DFT calculation (VA-KSO) slightly improved the agreement, but still cannot reproduce the intensity in the low momentum region. Note that the experimental distributions of HOMO depend on the impact energy. The intensity in the lower momentum region ($p < 0.5$ a.u.) at 1200 eV is lower than that at 600 eV. One possible explanation is the distorted-wave effect, which has been found in a few *d*-like molecular orbitals recently [15,16]. Dyson orbital of $2b_1$ in real space was also plotted in Fig. 2. Indeed, it has a pattern of two linked *d*-like orbitals. For those orbitals, the kinematic factor of the

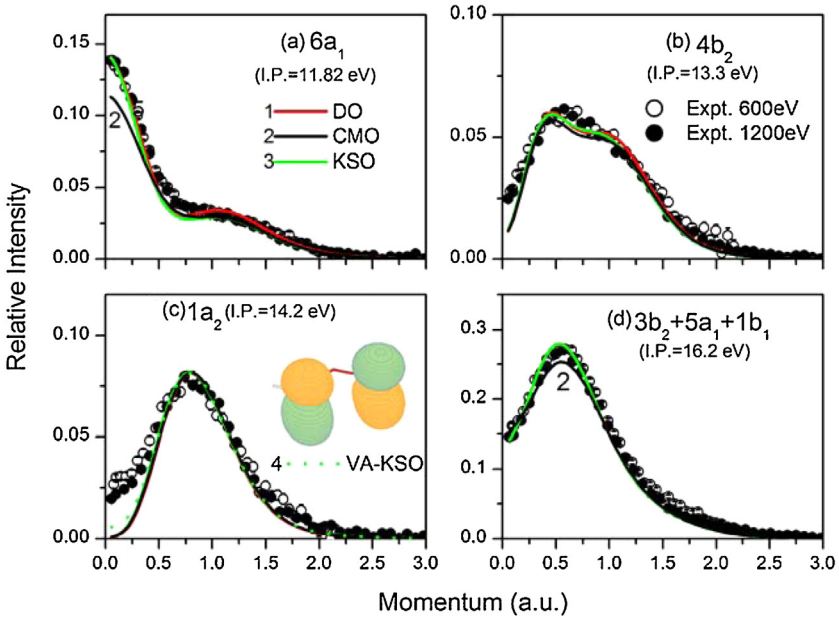

Fig. 3. Spherically averaged momentum distributions for $6a_1$, $4b_2$, $1a_2$, and $3b_2 + 1b_1 + 5a_1$ orbitals. The curves 1–3 are almost identical, so only one curve is visible. The curve 4 is the vibrationally averaged DFT calculation. The theoretical results have been convoluted with the experimental momentum resolution. The inset in (c) is the Dyson orbital of $1a_2$ plotted with a contour value 0.05.

differential (e, 2e) cross-section is no longer a constant. It depends on the impact energies and the molecular structures. PWIA is no longer a good approximation. Physically, such an effect is due to the non-negligible influence of nuclei on the incident electrons or scattered electrons. Moreover, the de Broglie wavelength of scattered electrons with a kinetic energy of 300 eV is 0.71 Å, 0.50 Å for 600 eV, which are comparable with bond length d_{CO} = 1.41 Å. Therefore, electron diffraction is one possible mechanism that changes the momentum distributions. Electron diffraction has been experimentally observed and theoretically predicted in the photoelectron angular distributions using X-ray or synchrotron radiation [38,39]. The symmetric molecular structure and the anti-symmetric molecular orbital, which has zero intensity at the momentum origin, may make the effects more noticeable.

Supplementary material related to this article can be found, in the online version, at http://dx.doi.org/10.1016/j.elspec.2014.01.019.

In Fig. 3(a), KSO and DO reproduce the experimental momentum distributions of $6a_1$ orbital very well. However, CMO underestimated the observed intensity in the low momentum region, which agrees with Zheng et al. [11]. Fig. 3(b) shows the momentum distributions of $4b_2$. The three models can describe the experimental distributions except the discernible difference below the momentum of 0.2 a.u. The experimental momentum distributions

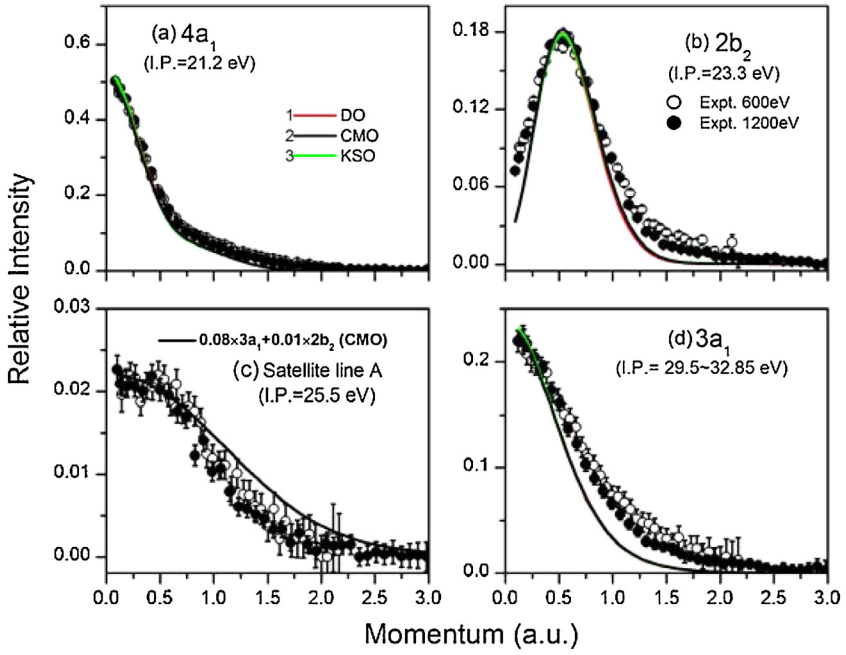

Fig. 4. Spherically averaged momentum distributions for $4a_1$, $2b_2$, the satellite line A, and $3a_1$. The curves 1–3 are almost identical, so only one curve is visible. The theoretical results have been convoluted with the experimental momentum resolution.

of $1a_2$ were compared with calculated ones in Fig. 3(c). The overall shapes of calculated distributions agree with the observed results. However, all calculations underestimate the experimental intensity in the low momentum region. In the previous work, Zheng et al. [11] observed remarkable discrepancies between the experimental distributions and calculated ones for $4b_2$ and $1a_2$ orbitals individually, which was ascribed by authors to their poor energy resolution 1.3 eV. And, they obtained much better agreement by comparison of the summed theoretical and experimental momentum distributions of $4b_2 + 1a_2$. The deconvolution procedure may not be able to extract the individual contribution cleanly because of the significant overlap in Fig. 1(a). However, in the present work, it cannot explain why the predicted intensity in low momentum region is evidently lower than the observed ones for $1a_2$. Since the momentum distributions of DO, KSO, CMO are almost identical, the discrepancy is not likely due to electron correlation effects. Again, we found that the nuclear vibration effect (mainly ν_{11} mode, 1482 cm^{-1}) cannot explain the observed distributions although it has non-neglectable effects on the momentum distributions of $1a_2$. It is interesting to note that $1a_2$ is a d-like orbital. The discrepancy may be still due to non-negligible effects of nuclei, which is similar to the case of HOMO. Indeed, the experimental momentum distributions of 600 eV show a difference from that of 1200 eV although not remarkable. In Fig. 3(d), the calculated distributions of DO and KSO are in excellent agreement with the experimental distributions of $3b_2 + 5a_1 + 1b_1$. However, CMO underestimated the maximum intensity. The comparison in Fig. 3(a) and (d) showed that the electron correlation effects are important for accurately calculating the momentum distribution.

In Fig. 4(a), DO, CMO, and KSO reproduce the experimental distributions of 4a1 orbital very well. In Fig. 4(b), the three types of calculations can describe the overall shapes of experimental distributions, but they predicted narrower momentum distributions than the observed distributions. Fig. 4(c) shows the experimental momentum distributions of band A at 25.5 eV (see Fig. 1(a)), which cannot be reproduced by the high-level SAC-CI theory. To tentatively explain the observed momentum distributions, a linear combination of $3a_1$ and $2b_2$ CMOs was used to describe the experimental distributions. The coefficients were determined for the best fitting. It is not clear why SAC-CI cannot predict band A. It may be due to the truncated active space we used. The full active space calculation is too expensive and beyond our ability. Another possible reason is the dissociative ionization, which was not considered in the SAC-CI calculation. The energy spectra related to the dissociative ionization are usually every broad. One typical example is excitation-ionization of H_2 [40]. In Fig. 4 (d), three types of calculations can reproduce the overall experimental profile of the broad band at 32 eV, which is mainly composed of the $3a_1$ orbital and its satellite lines.

4. Conclusions

The valence electronic structures of dimethyl ether were investigated using the high-resolution electron momentum spectroscopy at 600 and 1200 eV in combination with the various theoretical calculations. In general, the observed binding energy spectra and momentum distributions can be well described using SAC-CI and DFT methods. It was found that the nuclear ground vibrational motions have non-neglectable effects on the momentum distributions of $2b_1$ and $1a_2$ orbitals. The discrepancies between the experimental distributions and the theoretical predictions of $2b_1$ and $1a_2$ orbitals in the low momentum regions may be due to non-negligible influence of nuclei on the incident electrons or scattered electrons.

Acknowledgments

This work was supported by the National Natural Science Foundation of China (11074144 and 11174175) and Tsinghua University Initiative Scientific Research Program.

References

[1] B. Boudaïffa, P. Cloutier, D. Hunting, M.A. Huels, L. Sanche, Science 287 (2000) 1658.
[2] C.J. Colyer, S.M. Bellm, B. Lohmann, G.F. Hanne, O. Al-Hagan, D.H. Madison, C.G. Ning, J. Chem. Phys. 133 (2010) 124302.
[3] S. Xu, H. Chaluvadi, X. Ren, T. Pfluger, A. Senftleben, C.G. Ning, S. Yan, P. Zhang, J. Yang, X. Ma, J. Ullrich, D.H. Madison, A. Dorn, J. Chem. Phys. 137 (2012) 024301.
[4] A.W. Potts, T.A. Williams, W.C. Price, Faraday Discuss. 54 (1972) 104.
[5] G. Bieri, L. Asbrink, W. von Niessen, J. Electron Spectrosc. Relat. Phenom. 27 (1982) 129.
[6] K. Kimura, S. Katsumata, Y. Achiba, T. Yamazaki, S. Iwata, Handbook of HeI Photoelectron Spectra of Fundamental Organic Molecules, Japan Scientific Societies Press, Tokyo, 1981.
[7] A. Schweig, W. Thiel, Mol. Phys. 27 (1974) 265.
[8] H. Bock, P. Mollere, G. Becker, G. Fritz, J. Organomet. Chem. 61 (1973) 113.
[9] S. Cradock, R.A. Whiteford, J. Chem. Soc., Faraday Trans. 2 (1971) 281.
[10] S.A.C. Clark, A.O. Bawagan, C.E. Brion, Chem. Phys. 137 (1989) 407.
[11] Y. Zheng, E. Weigold, C.E. Brion, W. von Niessen, J. Electron Spectrosc. Relat. Phenom. 53 (1990) 153.
[12] X.G. Ren, C.G. Ning, J.K. Deng, S.F. Zhang, G.L. Su, F. Huang, G.Q. Li, Rev. Sci. Instrum. 76 (2005) 063103.
[13] C.G. Ning, S.F. Zhang, J.K. Deng, K. Liu, Y.R. Huang, Z.H. Luo, Chin. Phys. B 17 (2008) 1729.
[14] E. Weigold, I.E. McCarthy, Electron Momentum Spectroscopy, Kulwer Academic Press, New York, 1999.
[15] C.G. Ning, X.G. Ren, J.K. Deng, G.L. Su, S.F. Zhang, G.Q. Li, Phys. Rev. A 73 (2006) 022704.
[16] X.G. Ren, C.G. Ning, J.K. Deng, S.F. Zhang, G.L. Su, F. Huang, G.Q. Li, Phys. Rev. Lett. 94 (2005) 163201.
[17] R.K. Singh, J.V. Ortiz, M.K. Mishra, Int. J. Quantum Chem. 110 (2010) 1901.
[18] C.M. Oana, A.I. Krylov, J. Chem. Phys. 127 (2007) 234106.
[19] M. Yamazaki, T. Horio, N. Kishimoto, K. Ohno, Phys. Rev. A 75 (2007) 032721.
[20] M.E. Casida, D.P. Chong, Int. J. Quantum Chem. 40 (1991) 225.
[21] P. Duffy, D.P. Chong, M.E. Casida, D.R. Salahub, Phys. Rev. A 50 (1994) 4707.
[22] H. Nakatsuji, Chem. Phys. Lett. 59 (1978) 362.
[23] M. Ehara, Y. Ohtsuka, H. Nakatsuji, M. Takahashi, Y. Udagawa, J. Chem. Phys. 122 (2005) 234319.
[24] C.W. Huang, X. Shan, Z. Zhang, E. Wang, Z. Li, X.J. Chen, J. Chem. Phys. 133 (2010) 124303.
[25] Q.G. Tian, J.Y. Shi, Y.F. Shi, X. Shan, X.J. Chen, J. Chem. Phys. 136 (2012) 094306.
[26] Y.R. Miao, C.G. Ning, K. Liu, J.K. Deng, J. Chem. Phys. 134 (2011) 204304.
[27] Y.R. Miao, C.G. Ning, J.K. Deng, Phys. Rev. A 83 (2011) 062706.
[28] Y.R. Miao, J.K. Deng, C.G. Ning, J. Chem. Phys. 136 (2012) 124302.
[29] C.G. Ning, X.G. Ren, J.K. Deng, G.L. Su, Z.F. Zhang, S. Knippenberg, M.S. Deleuze, Chem. Phys. Lett. 421 (2006) 52.
[30] A.D. Becke, J. Chem. Phys. 98 (1993) 5648.
[31] C. Lee, W. Yang, R.G. Parr, Phys. Rev. B 37 (1988) 785.
[32] W. von Niessen, J. Schirmer, L.S. Cederbaum, Comput. Phys. Rep. 1 (1984) 57.
[33] J.V. Ortiz, J. Chem. Phys. 89 (1988) 6348.
[34] P.R.T. Schipper, O.V. Gritsenko, S.J.A. vanGisbergen, E.J. Baerends, J. Chem. Phys. 112 (2000) 1344.
[35] D.P. Chong, J. Electron Spectrosc. Relat. Phenom. 184 (2011) 164.
[36] D.E. Woon, T.H. Dunning, J. Chem. Phys. 98 (1993) 1358.
[37] N. Watanabe, M. Yamazaki, M. Takahashi, J. Chem. Phys. 137 (2012) 114301.
[38] X. Guan, E.B. Secor, K. Bartschat, B.I. Schneider, Phys. Rev. A 85 (2012) 043419.
[39] A. Landers, Th. Weber, I. Ali, A. Cassimi, M. Hattass, et al., Phys. Rev. Lett. 87 (2001) 013002.
[40] S. Bellm, J. Lower, E. Weigold, D.W. Mueller, Phys. Rev. Lett. 104 (2010) 023202.
[41] Gaussian03 Revision E.01, Gaussian Inc., Wallingford, CT, 2004.
[42] ADF 2008.01, SCM, Theoretical Chemistry, Vrije Universiteit, Amsterdam, The Netherlands, 2008.